Statistical properties of armored gravel bed surfaces

J. Aberle[1] and V. Nikora[2]

Received 18 October 2005; revised 12 July 2006; accepted 9 August 2006; published 18 November 2006.

[1] Roughness of successively developed armor layers in a large laboratory flume is analyzed considering gravel surfaces as two-dimensional random fields of bed elevations. Statistically derived roughness parameters are evaluated from precise digital elevation models (DEMs) of bed surfaces and are discussed with respect to successive development of stable armor layers. The key results relate to evolution of the probability distribution of bed elevations and its moments and structure functions of various orders with respect to armoring discharge. Our results suggest that statistical analysis of bed elevations is a helpful tool for defining roughness parameters, quantifying armoring effects, and identifying particle orientation, flow direction, and surface-forming processes.

Citation: Aberle, J., and V. Nikora (2006), Statistical properties of armored gravel bed surfaces, *Water Resour. Res.*, *42*, W11414, doi:10.1029/2005WR004674.

1. Introduction

[2] The accurate description of armor layer roughness in rivers is of fundamental importance for fluvial geomorphology and river hydraulics since it determines such flow properties as mean flow velocity, turbulence, and sediment transport. Energy losses caused by multiscale bed roughness can be broadly subdivided into losses due to particle and form roughness [e.g., *Griffiths*, 1989]. Energy losses due to form roughness are mainly caused by large-scale roughness elements (or bed forms) and associated form drag. Energy losses due to particle roughness, on the other hand, result from viscous drag on the bed surface and form drag due to small-scale roughness elements such as grains of the bed material. These losses depend on particle size, shape, and arrangement [*Schlichting and Gersten*, 1997].

[3] Traditionally, particle roughness in gravel bed rivers is associated with a characteristic grain size of the bed material (e.g., d_{50}, d_{84}, or d_{90}). Such percentiles of particle size distributions can be evaluated from laboratory sieve analysis or using *Wolman's* [1954] sampling method or *Fehr's* [1987] line-by-number procedure in field studies. A recent comparison of various methods is given in the work of *Bunte and Abt* [2001]. The basic idea of using a single characteristic grain size as a roughness parameter goes back to the fundamental work of *Nikuradse* [1933]. The equivalent sand roughness k_s for gravel bed rivers can be roughly estimated as d_{50}, d_{84}, or multiples of these characteristic grain sizes [e.g., *Hey*, 1979; *Bathurst*, 1985; *Graf*, 1991; *Wiberg and Smith*, 1991]. However, gravel bed roughness in natural streams can be adequately described by a single characteristic percentile d only if the shape of the particle size distribution, bed arrangement, particle shape and orientation, packing, spacing and sorting, particle clusters, etc. are universal [*Nikora et al.*, 1998]. In other words, the use of d as a roughness parameter requires that independently formed gravel bed surfaces with the same d show exactly the same resistance to flow for identical hydraulic conditions. The abundance of flow resistance equations for gravel bed rivers, on the other hand, indicates that this is not the case, as many studies showed that bed structure may significantly affect the overall hydraulic resistance [*Bathurst*, 1978; *Bray*, 1982; *Furbish*, 1987; *Robert*, 1990; *Clifford et al.*, 1992; *Baiamonte and Ferro*, 1997; *Nikora et al.*, 1998; *Ferro*, 1999; *Aberle and Smart*, 2003; *Smart et al.*, 2004].

[4] An alternative way to take into account bed surface structure and to describe bed roughness is to consider the bed as a random field of surface elevations $Z(x,y,t)$, where x and y are longitudinal (main flow direction) and transverse coordinates, and t is time. Until the early nineties, only a few studies have considered gravel bed roughness following this approach by analyzing bed profiles [e.g., *Furbish*, 1987; *Robert*, 1988, 1990, 1991; *Clifford et al.*, 1992]. In recent years, this approach has become more popular due to technological advances in bed surface measurements such as photographic techniques and laser scanning methods [*Nikora et al.*, 1998; *Goring et al.*, 1999; *Butler et al.*, 2001; *Aberle and Smart*, 2003; *Marion et al.*, 2003; *Nikora and Walsh*, 2004; *Smart et al.*, 2004]. These advances also stimulated the development of methods for representing complex surface topography in high-resolution three-dimensional computational fluid dynamic models [e.g., *Lane et al.*, 2004; *Hardy et al.*, 2005; *Carney et al.*, 2006].

[5] In this paper we explore the applicability of the random field approach to describe the structure of successive water-worked, armored gravel bed surfaces using laboratory data. In addition to conventional statistical parameters such as standard deviation, skewness, and kurtosis coefficients, we apply second-order and higher-order structure functions to reveal statistical properties and potential multiscaling behavior of bed elevation fields. These parameters and methods are used to investigate the evolution of successively developed armor layers. Our

[1]Leichtweiss-Institute for Hydraulic Engineering, Technical University of Braunschweig, Braunschweig, Germany.
[2]Engineering Department, University of Aberdeen, Aberdeen, UK.

0043-1397/06/2005WR004674

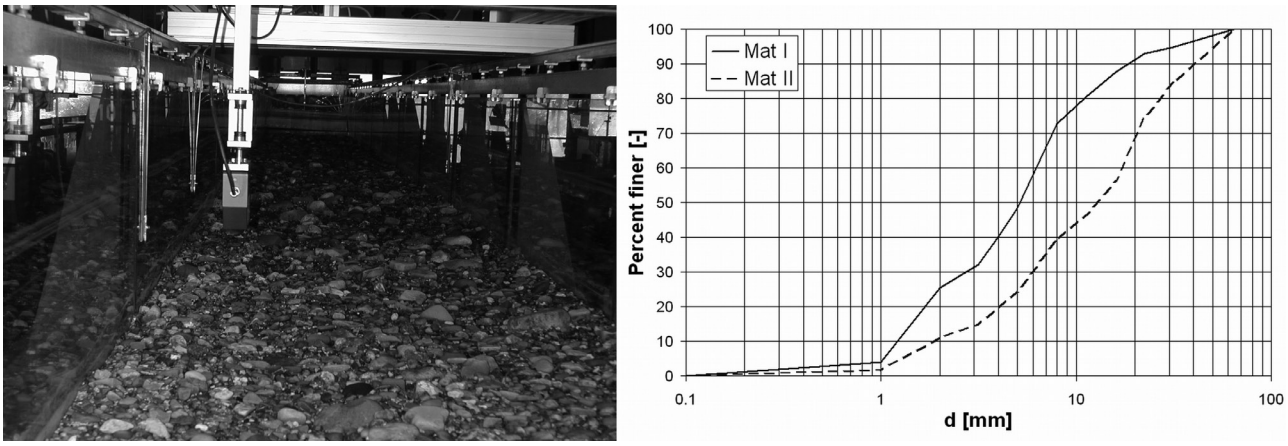

Figure 1. (left) View of the flume during laser scan and (right) grain size distributions of initial bed material.

target is the grain-scale range, from a few millimeters to the maximum bed particle size on the bed.

2. Data and Methods

[6] The gravel bed topography data analyzed in this paper were obtained from laboratory experiments in a 20 m long, 0.90 m wide and 0.60 m high tilting flume in the laboratory of the Leichtweiss-Institute for Hydraulic Engineering, Technical University of Braunschweig, Germany. These experiments were specifically designed to study the interaction between flow and roughness for flows with low and medium relative submergence [see *Aberle and Koll*, 2004; V. Nikora et al., Double averaging concept for rough-bed open-channel and overland flows: Theoretical background, submitted to *Journal of Hydraulic Engineering*, 2006, hereinafter referred to as Nikora et al., submitted manuscript, 2006a; also Double averaging concept for rough-bed open-channel and overland flows: Applications, submitted to *Journal of Hydraulic Engineering*, 2006, hereinafter referred to as Nikora et al., submitted manuscript, 2006b]. Two different coarse sediment mixtures with 0.63 mm $< d <$ 64 mm (see Figure 1 for grain size distributions) were used as movable bed material for the development of water-worked roughness structures.

[7] At the beginning of an experiment, the well-mixed sediment was placed in the flume over a length of 13.40 m and flattened to a thickness of 0.20 m to ensure that the bed surface was parallel to the flume plastic bottom. The distance from the flow straightener at the flume inlet to the sediment bed was 1.00 m and the gap between was bridged with bricks to avoid extensive scouring at the inlet. At the downstream end the sediment body was stabilized by a 0.20 m high sill. The sill was constructed of perforated metal to allow flow in the subsurface layer.

[8] The surface was allowed to armor for a given constant discharge Q_{a1} which was adjusted by a valve and measured by an inductive flowmeter. When the sediment transport rate became negligible, the discharge was reduced to zero and photographs of the armor layer were taken and analyzed by applying the line-by-number method of *Fehr* [1987] to obtain the grain size distribution of the armor layer. The method was calibrated by manually sampling the surface layer for a selected experiment and adjusting parameters so that differences between a sieve-based grain size distribution and a distribution from photographs were minimized. A detailed description of the applied method is beyond the scope of this paper, and further information on gravel size analysis from photographs and on statistical approaches to determine the grain size distribution from bed material surface samples is given, e.g., by *Adams* [1979], *Fehr* [1987], *Fraccarollo and Marion* [1995], and *Bunte and Abt* [2001].

Table 1. Summary of the Experimental Conditions[a]

Experiment	Mat	S_F	Q_a, L s^{-1}	τ_0, N m^{-2}	d_{50}, mm	d_{84}, mm	σ_z, mm	S_k	K_u	H_x
A	I	0.0027	0	-	5.2	13.5	1.5	−0.7	4.6	0.44
			120	5.2	11.1	27.2	4.8	0.5	3.3	0.61
			180	6.2	13.6	28.7	6.3	0.6	3.3	0.62
			220	7.0	18.4	44.4	8.2	0.8	3.9	0.63
			250_a	8.4	19.5	47.5	10.9	1.0	4.3	0.65
			250_b	8.6	19.6	48.4	10.8	1.0	4.2	0.64
B	I	0.0027	0	-	5.2	13.5	2.6	−0.2	3.6	0.47
			120	4.8	11.3	24.7	6.0	0.2	3.1	0.59
			180	6.3	15.3	32.4	7.7	0.8	4.6	0.62
			220	7.5	17.7	47.4	8.7	1.0	5.4	0.64
C	II	0.01	120	16.1	23.5	44.0	9.9	0.4	3.2	0.67
			180	20.5	25.0	48.8	12.6	0.7	3.4	0.67
			240	18.6	25.3	49.8	12.9	0.7	3.4	0.67

[a]Mat, initial bed material; S_F, flume slope; Q_a, armoring discharge; τ_0, bed shear stress; d_{50}, d_{84}, characteristic grain sizes; σ_z, standard deviation of bed elevations; S_k, skewness; K_u, kurtosis; H_x, scaling exponent. All values correspond to conditions at completion of armoring at the indicated water discharge Q.

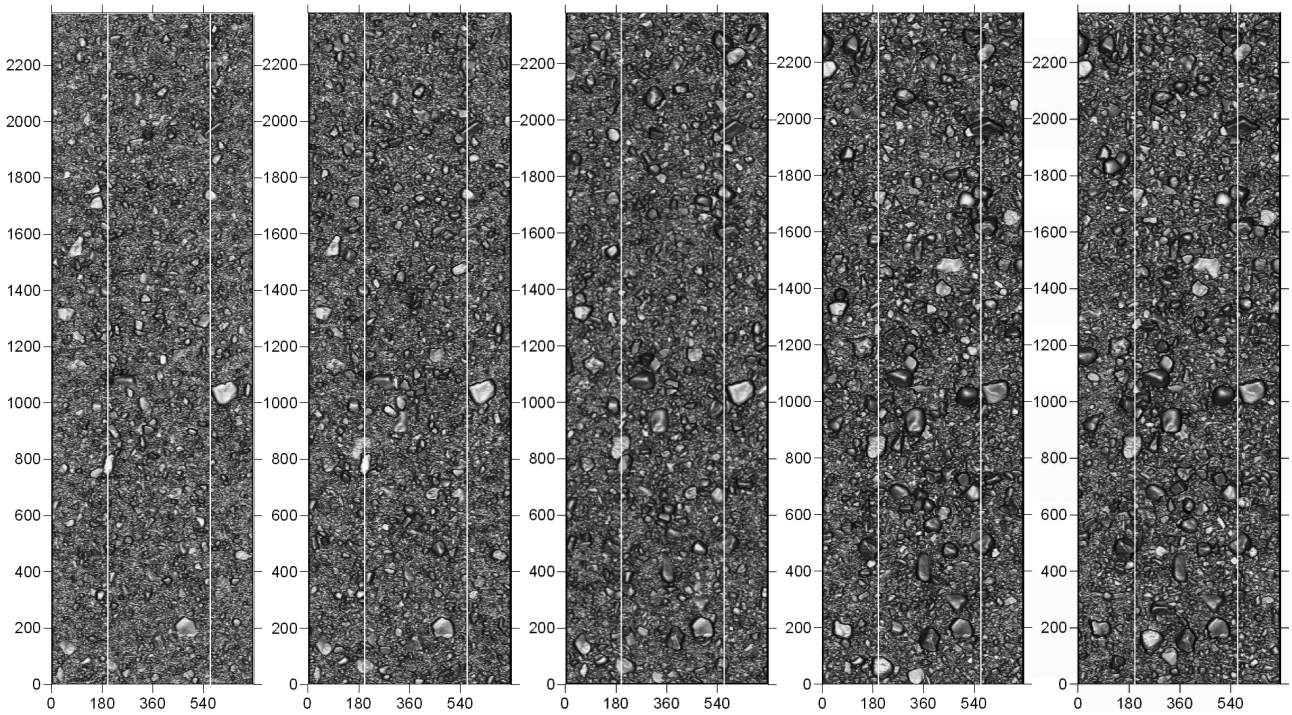

Figure 2. Digital elevation models shown as shaded relief maps after armoring with Q_a = 120, 180, 220, 250a, and 250b L s^{-1} for experiment A (from left to right). Flow direction is from the bottom to the top. Axis units are in mm.

[9] The bed topography was measured along the 2.40 m long test section with an Optimess laser displacement meter (Figure 1) over a width of 0.716 m. The test section was located 8 m from the transition bricks sediment so that neither the scour at the inlet section nor the downstream sill influenced the development of bed topography. Longitudinal bed profiles were recorded with a sampling interval of Δx = 1.0 mm with a lateral spacing between profiles of Δy = 4 mm, and with a vertical precision of ±0.1 mm. The different sampling intervals in x and y directions reflected the footprint of the sampling volume of the Optimess laser system (0.2 mm in flow direction and 4 mm in transverse direction). In total, 180 longitudinal profiles were recorded per surface scan.

[10] The bed survey was followed by velocity measurements made for the bed forming water discharge and for lower discharges with a Dantec three-dimensional (3-D) laser Doppler anemometer (LDA) to study the turbulent flow field over water-worked gravel surfaces. After the velocity measurements had been completed, the bed forming discharge Q_{a1} was increased to a value Q_{a2} (> Q_{a1}), so that the existing armor layer was destroyed and a new one developed. The above measurements were repeated and the procedure continued as long as the bed could stabilize itself without a considerable loss of slope or before the sediment was eroded to the plastic bottom of the flume. Table 1 summarizes available data for three experiments named A, B, and C and provides information on applied discharges and associated bed shear stresses. We note that for some of the experiments the armor layer was scanned a second time after the hydraulic measurements were finished. The analysis of these scans revealed no significant differences in armor layer geometry before and after the hydraulic measurements, and therefore these results are not presented here.

[11] All LDA measurements were carried out within the 2.40 m long and 0.364 m wide test section along the centerline of the flume to reduce sidewall effects. Therefore, in this paper we focus on this bed area in order to obtain bed surface characteristics which will be linked with turbulence characteristics in a follow-up study. Ninety-two longitudinal profiles in total were analyzed for each armor layer covering a strip approximately $6d_{max}$ wide. The detailed description of the hydraulic measurements is also beyond the scope of this paper as it focuses on the analysis of the topography data. Preliminary results of the hydraulic measurements are given by *Aberle and Koll* [2004] and Nikora et al. (submitted manuscript, 2006b).

[12] Before the DEMs were analyzed, the planar trend (which was chosen since bed forms were not present) was removed from the data using a least squares fit procedure. Figure 2 shows shaded relief plots of detrended surfaces for experiment A and corresponding armoring discharges Q_a of 120, 180, 220, 250_a, and 250_b L s^{-1}. The lines in each subplot indicate the width of the DEM sections used in the analysis below. It should be noted that the bed was armored twice at a discharge of 250 L s^{-1} because the bed was accidentally destroyed in a local upstream section during LDA measurements after the first armoring process (250_a L s^{-1}). Thus the bed was armored again and the corresponding armoring discharge was assigned index 250_b L s^{-1}.

[13] As a first step in our analysis, the detrended DEMs were used to estimate probability distribution functions (PDF) by removing the mean bed elevations first and then

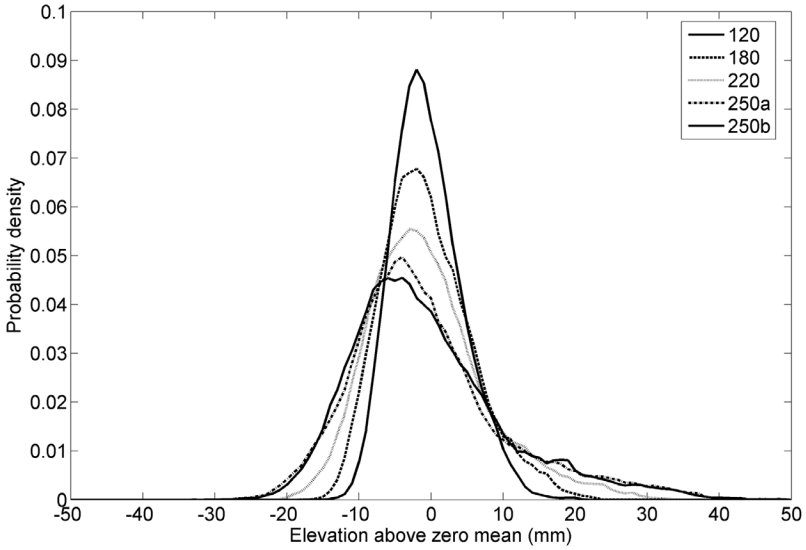

Figure 3. Probability distribution functions for armor layers at experiment A for Q_a = 120, 180, 220, 250_a, and 250_b L s^{-1}.

by building smoothed histograms using 100 bins, which cover the overall measuring range of the laser displacement meter of 100 mm (from −50 to +50 mm). The second step of our investigation of surface structure was the evaluation of moment functions. For this purpose we applied the generalized two-dimensional structure function as from *Nikora et al.* [1998] and *Nikora and Walsh* [2004]:

$$D_{Gp}(l_x, l_y) = \frac{1}{(N-n)(M-m)} \cdot \sum_{i=1}^{N-n} \sum_{j=1}^{M-m} \left\{ \left| z(x_i + n\delta x, y_j + m\delta y) - z(x_i, y_j) \right| \right\}^p \quad (1)$$

where $l_x = n\delta x$, $l_y = m\delta y$, δx and δy are the sampling intervals (1 and 4 mm, respectively), N and M are the total numbers of measuring points of bed elevations in x and y direction, and p is the order of the structure function.

[14] So far, most attention has been devoted to second-order structure functions (p = 2), which are identical to semivariograms [*Robert*, 1988, 1991; *Clifford et al.*, 1992; *Bergeron*, 1996; *Nikora et al.*, 1998; *Butler et al.*, 2001; *Marion et al.*, 2003]. The second-order structure function of a globally homogeneous random field has the following relationship with the correlation function $R(l_x, l_y)$:

$$D_{G2}(l_x, l_y) = 2\{\sigma_z^2 - R(l_x, l_y)\} \quad (2)$$

where σ_z is standard deviation of bed elevations.

[15] Thus, at large lags l_x and l_y when $R(l_x, l_y) \rightarrow 0$ and $D_{G2} \rightarrow 2\sigma_z^2$ the data are spatially uncorrelated and the corresponding lags l_x and l_y at which $D_{G2} \rightarrow 2\sigma_z^2$ may be used to derive characteristic longitudinal and transverse length scales [*Nikora et al.*, 1998].

3. Results and Discussion

[16] In the following sections we focus on the analysis of bed elevations $Z(x, y)$ with regard to the history of surface forming flow. All DEMs were obtained directly after each armoring step. Thus we focus on stable armor layers rather than on description of gravel bed geometry during the armoring process itself, as was done by *Marion et al.* [2003].

[17] We first consider the PDFs of bed elevations and their moments (e.g., variance, skewness, and kurtosis), and then we evaluate moment functions such as structure functions for the armored gravel bed surfaces.

3.1. Probability Distribution Functions and Their Moments

[18] Figure 3 shows the PDFs of bed elevations for the surfaces from Figure 2 for the different armoring discharges. Note that we omitted the PDF of the initially screeded bed since it is narrow and steep, with a maximum probability density of 0.31 for zero mean. From Figure 3 it follows that with rising armoring discharge the range of bed elevations increases and the number of observations around zero mean decreases. Thus the PDFs visualize the increase of geometrical roughness due to the accumulation of coarser grains on the surface during the successive armor layer development. The increased range of bed elevations can be quantified by the standard deviation of bed elevations σ_z (see Table 1), which can be interpreted as a characteristic vertical roughness length of gravel beds [*Nikora et al.*, 1998; *Aberle and Smart*, 2003]. Furthermore, the increased range of bed elevations becomes also apparent from the characteristic grain sizes d_{50} and d_{84} (Table 1).

[19] In Figure 4 we examine the relationship between σ_z, d_{50} and d_{84}. To compare our laboratory experiments with field measurements, Figure 4 also includes additional field data from New Zealand gravel bed rivers published by *Smart et al.* [2004]. Figure 4 reveals close relationships between σ_z and d_{50} and d_{84}. Both, the σ_z–d_{50} and σ_z–d_{84} plots show surprisingly little scatter of data points, while the field data follow the same trend as the laboratory data.

[20] In our earlier works [*Nikora et al.*, 1998; *Aberle and Smart*, 2003] we argued that the standard deviation σ_z of bed elevations is a better roughness scale compared to conventional d_{50} or d_{84}. Indeed, *Aberle and Smart* [2003]

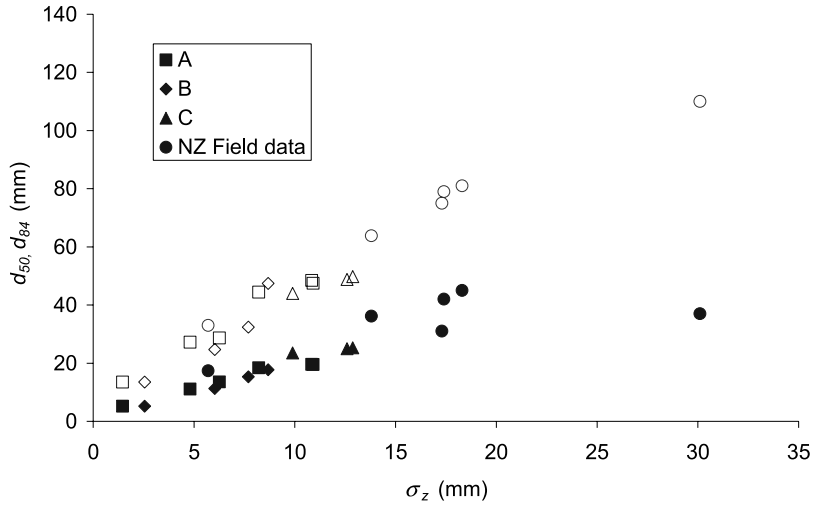

Figure 4. Standard deviation versus characteristic grain diameters d_{50} and d_{84}. The circles are for New Zealand field data from *Smart et al.* [2004]. The solid symbols characterize d_{50}, and the open symbols relate to d_{84}.

demonstrated that roughness of gravel beds with step pool morphology can be better described by σ_z compared to a characteristic grain size, which did not correlate with σ_z. Furthermore, *Aberle* [2000] and *Aberle and Smart* [2003] were able to show the superiority of σ_z over characteristic grain sizes in their resistance equation for steep gravel bed flows. *Vogel* [2003] confirmed the applicability of this flow resistance equation based on σ_z. The present study of armored gravel surfaces, however, reveals that σ_z and d_{50} (or d_{84}) are highly correlated, and therefore are equally suitable as measures of the roughness height. Figure 4 shows that this correlation is also applicable for field data of *Smart et al.* [2004]. The most plausible reason for this discrepancy is that in the present study and that of *Smart et al.* [2004] bed forms were not present and, as a consequence, the data from the flume and from the field closely collapsed. This result demonstrates that there are situations when the characteristic grain sizes may be as good roughness descriptors as σ_z. As our data show, one such situation corresponds to armored beds formed under conditions of a constant water discharge.

[21] A closer investigation of the PDFs shown in Figure 3 reveals that the shapes of the PDFs are not symmetrical. The data spread to the right of zero mean for the water worked beds and this spread is reflected by positive skewness S_k given in Table 1, which we directly relate to armoring effects. Only the initially screeded man-made beds (Q_a = 0 L s^{-1}) are characterized by negative skewness. In contrast to an initially screeded bed, the surface of an armored bed is composed of larger stones with finer particles filling depressions between them, thus reducing the magnitude of surface elevations below mean bed level. Therefore the PDFs are positively skewed [*Nikora et al.*, 1998; *Smart et al.*, 2004]. Table 1 shows that S_k values increase with armoring discharge, reflecting the accumulation of larger particles on the surface during successive armorings. One can also note that all measured PDFs are characterized by $K_u > 3$ (Table 1) indicating an increased (compared to the normal distribution for which $K_{u,N} = 3$) intermittency of bed elevations that can be attributed to the effect of rare large particles. Similar values for S_k and K_u for PDFs of longitudinal and transverse profiles of water-worked beds in gravel bed rivers have been reported by *Nikora et al.* [1998].

[22] All higher statistical moments (σ_z, S_k, K_u) show a high degree of reproducibility for experiments A and B, which have been carried out with the same bed material and armoring discharges. However, a closer examination of σ_z, S_k, K_u values given in Table 1 indicates that for similar discharges, all three moments are larger for experiment B compared to experiment A. Two possible explanations can be given for this behavior. First, the initial beds were prepared by different persons and thus the characteristics of the initial sediment bodies (e.g., compactness) may have been slightly different. Another possible explanation is that after the initial bed of experiment A was prepared and armored with Q_a = 120 L s^{-1}, more than half a year passed before the next armoring discharge Q_a = 180 L s^{-1} was applied. During this period, the 3-D LDA and a new traverse system were installed to the flume and hydraulic measurements have been carried out with an Acoustic Doppler Velocimeter (ADV) at various discharges equal and smaller than the armoring discharge [*Aberle and Koll*, 2004]. The DEM for Q_a = 120 L s^{-1} for experiment A used in this study was obtained directly before the LDA measurements were carried out. Thus the bed could settle for more than half a year before the surface was scanned while for all other armoring steps the surface was scanned directly after armoring. Therefore the differences in statistical parameters for experiments A and B for identical discharges may be attributed to additional compaction of the bed.

[23] Table 1 also shows that σ_z, S_k, and K_u do not change from armoring step of 180 to 240 L s^{-1} for experiment C, although the bed stabilized itself again during the armoring process. We associate this behavior with bed degradation, which became apparent from the planar fit parameters of the surface and the water surface slope. The slope reduction indicates that the critical shear stress for the mixture, which corresponds to the armor layer, has been reached between Q_a = 180 and 240 L s^{-1}. Once this critical shear stress is

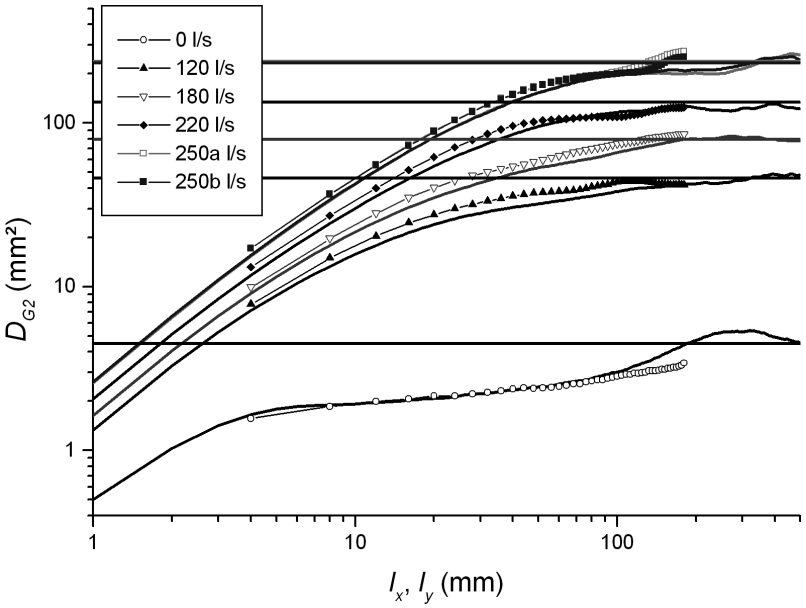

Figure 5. Second-order structure functions for $l_y = 0$ (straight lines) and $l_x = 0$ (line and symbol) for the surfaces shown in Figure 2 and for the initial bed (Q_a = 0 L s^{-1}). The horizontal lines indicate the corresponding values of $2\sigma_z^2$.

exceeded, the bed can only stabilize again by degradation of the bed slope [*Günter*, 1971], which is associated with a reduction of bed shear stress as indicated by τ_0 values given in Table 1.

[24] Applying the Kolmogorov-Smirnov test to the data showed that the hypothesis of a normal distribution must be rejected at significance levels of 0.05 and 0.01 for all PDFs under investigation, due to the increased skewness and kurtosis coefficients. *Smart et al.* [2004] concluded that skewed distributions of natural gravel bed surfaces may well be fitted by a lognormal frequency distribution. However, as for the normal distribution, our analysis showed that the hypothesis of a lognormal distribution must be also rejected. Hence, although all PDFs are bell shaped and may be considered as near-Gaussian, the positive skewness coefficients and high kurtosis coefficients are the main reason for the rejection of the hypothesis of a normal or lognormal distribution.

3.2. Second-Order Structure Functions

[25] In Figure 5 we present second-order structure functions according to (1) for the surfaces shown in Figure 2. The line graphs show $D_{G2}(l_x, l_y = 0)$, the line and symbol graphs show $D_{G2}(l_x = 0, l_y)$, and the straight lines define $2\sigma_z^2$ for the corresponding surface.

[26] The second-order structure functions follow the pattern that has been observed in various investigations focusing on the analysis of longitudinal and transverse bed profiles [*Robert*, 1988, 1991; *Nikora et al.*, 1998] as well as surfaces [*Butler et al.*, 2001; *Nikora and Walsh*, 2004]. The region at small spatial lags, where the structure functions can be approximated by power functions $D_{G2} \propto l^{2H}$, corresponds to the scaling region, while at large lags the structure functions approach the saturation region with $D_{G2}(\infty) = 2\sigma_z^2$. The scaling exponent H is known as the Hurst exponent and estimates of H_x are presented in Table 1. Between these two regions, the structure functions are curved in the so-called transition zone [*Nikora et al.*, 1998; *Nikora and Walsh*, 2004].

[27] Bearing this separation zone in mind, Figure 5 provides important information on surface structure and scaling intervals. The extent of the scaling region increases with rising armoring discharge and for our data, the upper limit for the extent of the scaling region may be defined within $l_x/d_{50} < 0.5$. Furthermore, the data in Table 1 show a dependency of the scaling exponents H_x on armoring discharge and subsurface material. Beds armored at higher discharges are characterized by larger scaling exponents H_x and largest H_x values are observed for experiment C, which has been carried out with the rougher material II. The scaling exponent H_x can be interpreted as a measure of complexity of topography, where larger values of H_x indicate a less complex topography [*Bergeron*, 1996]. Increasing H_x values with armoring discharge can therefore be explained by the fact that the smooth surface of large individual particles creates a less complex topography than a large number of small particles. These results support the observations of *Robert* [1988] and *Bergeron* [1996], that gravel bed rivers seem to be smoother at the scaling range when the surface is composed of large particles. Our estimated H_x values for water-worked beds range from 0.59 to 0.67, and these values are in the same range as those reported by *Nikora et al.* [1998], *Butler et al.* [2001], and *Nikora and Walsh* [2004] for field and flume studies. Thus the scaling exponent for gravel bed surfaces seems to be in a narrow range although our data also suggest its dependence on grain geometry.

[28] While the data density is large enough in the flow direction (δx = 1 mm) to evaluate the scaling exponents H_x using $D_{G2} \propto l^{2H_x}$, Figure 5 shows that the data density in the transverse direction (δy = 4 mm) is not large enough for a reliable estimation of H_y. For all structure functions the second data point of $D_{G2}(l_x = 0, l_y)$, which corresponds to a

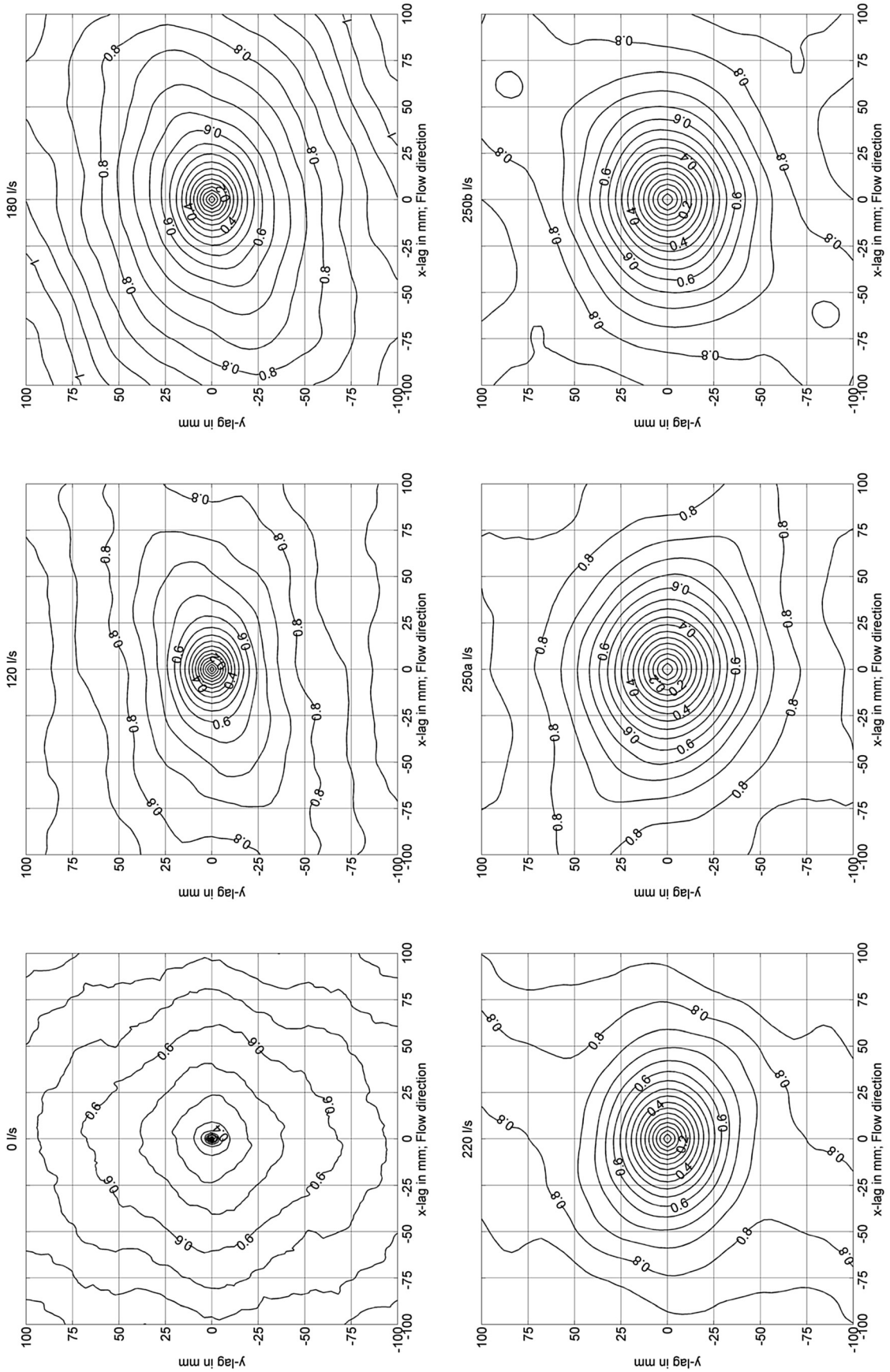

Figure 6. Contour plots of the second-order structure functions for surfaces at experiment A armored with $Q_a = 0$, 120, 180 L s^{-1} (top, from left to right), and 220, 250$_a$, 250$_b$ (bottom, from left to right).

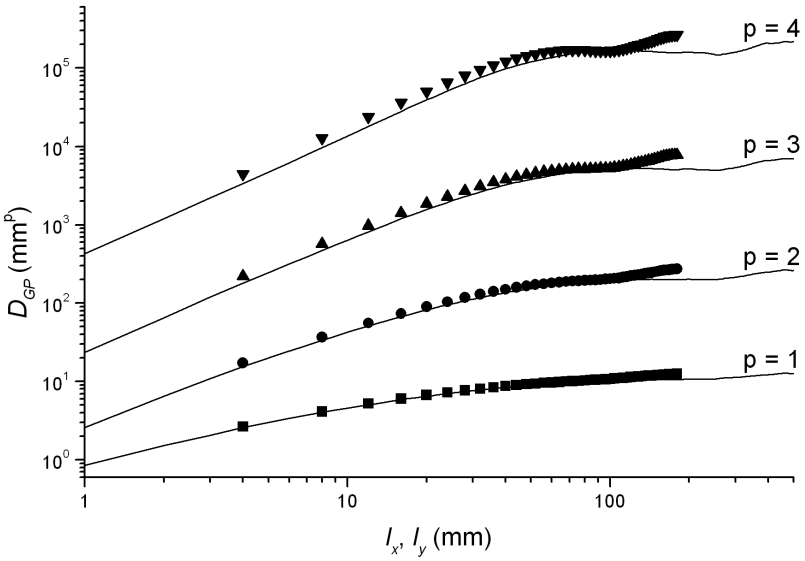

Figure 7. Higher-order structure functions (p = 1 – 4) for $l_y = 0$ (lines) and $l_x = 0$ (symbols) for the gravel surface armored with $Q_a = 250_a$ L s^{-1}.

lag of 8 mm, is already located in the transition zone. A direct comparison of $D_{G2}(l_x, l_y = 0)$ and $D_{G2}(l_x = 0, l_y)$ for the same surfaces shows that the shapes of the curves are similar, although the curves are separated by a small offset [$D_{G2}(l_x = 0, l_y) > D_{G2}(l_x, l_y = 0)$]. The studies of *Nikora et al.* [1998], *Butler et al.* [2001] and *Nikora and Walsh* [2004] indicate that scaling is isotropic at small spatial lags, i.e., $H_x = H_y$. Such an assumption may be deduced from the parallel lines of $D_{G2}(l_x = 0, l_y)$ and $D_{G2}(l_x, l_y = 0)$ in the log-log coordinates. The observed vertical offset between $D_{G2}(l_x = 0, l_y)$ and $D_{G2}(l_x, l_y = 0)$ is consistent with shape of the two-dimensional second-order structure functions $D_{G2}(l_x, l_y)$.

[29] The plots of $D_{G2}(l_x, l_y)$ are useful to identify isotropy/anisotropy of the random field [*Butler et al.*, 2001; *Nikora and Walsh*, 2004] and are given in Figure 6 for surfaces shown in Figure 2. All contour lines in Figure 6 are normalized with $2\sigma_z^2$ to enable a direct comparison of the plots during successive armor layer development. The maximum spatial lag shown in both x and y direction has been chosen as ±100 mm, being larger than the maximum particle size of 64 mm. The contour lines for all water-worked beds ($Q_a > 0$ L s^{-1}) are characterized, at relatively small spatial lags, by an elliptical shape. Geometrically, the elliptical shape of the contour lines reflects the elliptical form of the particles. The contour minor axis is aligned with the prevailing orientation of the b (intermediate) axis of the particles and the major axis with the orientation of the a (largest) axis of the particles. Figure 6 shows that the longest axes of the elliptical contours of $D_{G2}(l_x, l_y)$ at small spatial lags are aligned in flow direction indicating that the majority of particles tend to rest on the bed with their longest axis along the flow. In our study, the constant water discharge was applied until the transport rate became negligible. At this later stage of armoring, smaller particles were not rolling anymore as the applied bed shear stress became close to the critical bed shear stress. Instead, the particles responded to the flow by aligning their longest axis in the flow direction before they finally rested, at armoring completion. This hypothesis of particle alignment finds support in qualitative observations of *Allen* [1982]. On the other hand, large particles that did not move during armoring were arbitrarily orientated. This explains misalignment of larger elliptical contours of $D_{G2}(l_x, l_y)$ from the flow direction (Figure 6).

[30] If the applied bed shear stress would suddenly reduce during active bed load with rolling particles then they would rest on the bed with longest axes across the flow, i.e., differently to our case study. The elliptical contour lines of the structure functions corresponding to this case would also have their longest axis across the flow. Such a scenario has been discussed by *Komar and Li* [1986], *Robert* [1991], *Nikora et al.* [1998], *Butler et al.* [2001], and *Nikora and Walsh* [2004]. There may be even more complex particle arrangements such as, for instance, diamond-shaped clusters. In this later case the 2-D structure functions should also exhibit diamond-shaped topography oriented along the flow direction. It should be also noted that there are always particles on the bed deviating from the overall rule, depending on grain shape and position within particle clusters [*de Jong*, 1995]. Thus our results confirm the findings of *Butler et al.* [2001] and *Nikora and Walsh* [2004] that the structure functions of bed elevation provide useful information on the history of surface-forming mechanisms for the water-worked gravel beds.

[31] Figure 6 further reveals that the elliptical contour lines for $D_{G2}(l_x, l_y)/(2\sigma_z^2) < 0.5$ are growing in size for the water-worked beds with increasing armoring discharge. Bearing in mind that the shape of the contour lines reflects particle geometry, the expansion of the contour lines shows that during successive armor layer development an increasing number of coarse particles forms the surface, while finer material is washed out (see Figure 2). In Figure 6 the main axis of the ellipse formed by the contour line $D_{G2}(l_x, l_y)/(2\sigma_z^2) = 0.5$ increases from $l_x = 18$ mm at $Q_a = 120$ L s^{-1} to $l_x = 33$ at $Q_a = 250_b$ L s^{-1}. The minor axis increases correspondingly from $l_y = 15$ mm to $l_y = 28$, still being smaller than maximum particle size of 64 mm. Similar results were observed for experiments B and C.

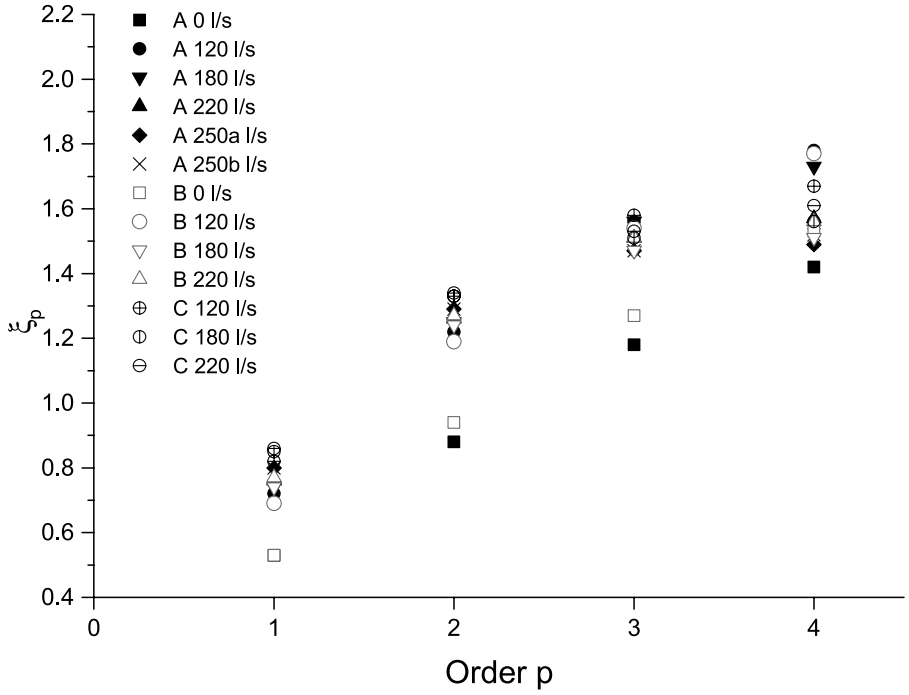

Figure 8. Scaling exponents versus structure function order.

[32] For the initial bed of experiment A, the contour lines of $D_{G2}(l_x, l_y)$ at very small spatial lags are circular, indicating at isotropy of the surface structure. However, the data for experiment B demonstrate the elliptical contours. We associate the differences in contour shape with bed preparation, since different persons prepared the initial beds. Note that for experiment C no initial scan is available due to a corrupted data file.

3.3. Higher-Order Structure Functions

[33] *Nikora and Walsh* [2004] recently investigated higher-order structure functions ($p = 1 - 6$) of gravel bed surfaces of New Zealand rivers studied in the work of *Smart et al.* [2004]. The higher-order structure functions provide additional information on scaling behavior of water-worked gravel surfaces. In Figure 7 we show structure functions for orders $p = 1 - 4$ for experiment A with $Q_a = 250_a$. Similar to the second-order structure functions, the higher-order structure functions can also be subdivided into a scaling region, a transition region, and a saturation region. The nearly constant value of the structure functions in the saturation region indicates that the data are statistically homogeneous.

[34] There are two types of scaling that can be identified using high-order structure functions: simple scaling corresponds to $\xi_p = Hp$ while for multiscaling $\xi_p \neq Hp$, where ξ_p is the scaling exponent for the scaling region ($D_{Gp} \propto l_x^{\xi p}$). Thus the scaling behavior may be identified by plotting the exponents ξ_p versus order p of the structure functions [*Nikora and Walsh*, 2004]. Such a plot, shown in Figure 8, indicates that the initial beds are characterized by simple-scaling behavior while the water-worked beds more likely relate to multiscaling. Indeed, with increase in p the deviation of ξ_p from a linear relation increases indicating multiscaling of water-worked gravel beds. Similar results were obtained by *Nikora and Walsh* [2004]. The origin of multiscaling behavior in gravel surfaces may relate to surface forming processes [e.g., *Nikora*, 2005]. However, we also have to keep in mind potential effects of data acquisition, resolution, and detrending, which smooth the real topography and may bias scaling exponents ξ_p. Proper evaluation of these effects requires highly accurate and extensive data sets, which have not been available yet to the writers.

3.4. Determination of Flow Direction

[35] As we pointed out above, the elliptical contours of the surface plots of the second-order structure functions may indicate a flow orientation. However, they do not reveal flow direction, i.e., from left to right or from right to left. A possible approach for identifying flow direction is to use local bed inclinations at small spatial lags [*Monzavi*, 1972; *Smart et al.*, 2004] by defining an average positive bed slope:

$$\varepsilon_p(l) = \frac{1}{n_p}\sum_{i=l}^{n_p}\left[\frac{z(x_i + l_x) - z(x_i)}{l_x}\right] \qquad z(x_i + l) - z(x_i) > 0 \tag{3}$$

and average negative bed slope

$$\varepsilon_n(l_x) = \frac{1}{n_n}\sum_{i=l}^{n_n}\left[\frac{z(x_i + l_x) - z(x_i)}{l_x}\right] \qquad z(x_i + l_x) - z(x_i) < 0 \tag{4}$$

where n_p and n_n are total numbers of positive and negative slopes, respectively. Note that relationships (3) and (4) are similar to the sign-specific structure functions based on increments of the same sign [*Nikora et al.*, 1994; *Frisch*, 1995].

[36] Our data show that $\varepsilon_p < |\varepsilon_n|$ for small lags l_x except for experiment A and $Q_a = 120$ L s^{-1} where ε_p is slightly

larger than ε_n for $l_x = 1$ mm and $\varepsilon_p < |\varepsilon_n|$ for lags 2 mm $< l_x <$ 8 mm. This result may be associated with the aforementioned bed aggregation, although the second scan directly after the LDA measurements revealed that $\varepsilon_p < |\varepsilon_n|$ throughout. We note that standard deviations σ_z of the two scans could be interpreted as identical when tested for equality at a significance interval of 0.01 using the procedure outlined by *Kreyszig* [1991] for identical variances of two non-Gaussian distributions.

[37] At small lags $\varepsilon_p < |\varepsilon_n|$ is expected [*Monzavi*, 1972; *Smart et al.*, 2004; *Nikora and Walsh*, 2004], because negative increments of surface elevations in flow direction have higher magnitudes than positive slopes due to particle imbrication and arrangement. We found that at small lags, negative slopes are less frequent than positive slopes as was described by *Smart et al.* [2004] and *Nikora and Walsh* [2004].

4. Summary and Conclusions

[38] Previous studies of armor layer development have been restricted to interpretation of grain size distributions at various stages and the roughness of armor layers has been described by characteristic grain diameters. This paper investigates, for the first time, armor layer geometry of successively developed stable armor layers by means of statistical parameters, which were obtained from digital elevation models. The key findings of the study include: (1) the characteristic vertical roughness length of gravel beds may be unambiguously defined by the standard deviation of bed elevations σ_z, (2) the PDFs of water-worked gravel beds are sensitive to bed armoring suggesting that skewness and kurtosis coefficients can be used for quantifying armoring effects; and (3) the coarsening of the surface during armor layer development as well as particle orientation can be effectively quantified using generalized structure functions of surface elevations.

[39] Relating σ_z to the applied armoring discharge showed that σ_z increases during successive armor layer development due to accumulation of coarser grains on the gravel bed surface. Furthermore, close relationships between σ_z and characteristic grain diameters d_{50} and d_{84} have been found for beds without bed forms and prominent clusters. Additional field data from New Zealand rivers, which follow the same relationship as the laboratory data, showed that these relationships are not flume related.

[40] All PDFs of all water-worked armor layers were found to be positively skewed which was related to the armoring process. During the armoring process, finer particles are settling in holes in the bed surface and thus reduce the magnitude of surface elevations below mean bed level, resulting in positive skewness coefficients. Furthermore, skewness coefficients were found to increase with armoring discharge which was associated with accumulation of coarser grains on the bed surface. Besides, kurtosis was always larger than for a normal distribution and the hypothesis of a Gaussian distribution of the PDFs could not be accepted, although the PDFs were bell-shaped.

[41] The coarsening of the bed surface was also observed in the second-order generalized structure functions of bed elevations. The scaling region at small spatial lags was found to be related to approximately $0.5d_{50}$ and the structure functions showed that the scaling region depends on armoring discharge. The scaling exponents H_x of $D_{G2}(l_x, l_y = 0)$, which can be interpreted as a measure of complexity of the surface, were as well found to increase with armoring discharge and to be dependent on subsurface bed material. The increase of scaling exponents with armoring discharge was explained by the fact that the smooth surface of large individual particles creates a less complex topography than a large number of small particles. All evaluated scaling exponents were found to be in a similar range as previously reported ones, indicating at similar scaling-forming mechanism for gravel bed surfaces at small lags. The 2-D generalized structure functions provided information and insight on the coarsening of the surface as well as particle arrangement. Smaller particles were found to be orientated with their longest axis in flow direction and this was reflected by ellipticity of contours of $D_{G2}(l_x, l_y)$. A method to identify flow direction by means of negative and positive local slopes was also proposed.

[42] The results of this study show that the random field approach for the description of bed roughness provides deeper insight into surface forming processes of gravel beds than is possible by conventional description of bed roughness and texture using characteristic grain sizes. The next step to enhance our understanding of relevant physical processes of the interaction of complex roughness and flow is to link statistical parameters with the turbulent flow field. The double averaging methodology, which is based on temporal and spatial averaging of the Navier-Stokes equation provides a theoretical background for such investigations. This methodology, which was recently revisited by Nikora et al. (submitted manuscript, 2006a; submitted manuscript, 2006b), requires detailed knowledge of surface geometry. This paper attempted to provide such knowledge.

Notation

d	grain diameter.
d_{50}, d_{84}	characteristic grain sizes.
D_{Gp}	generalized structure function of order p.
H_x	scaling exponent.
k_s	equivalent sand roughness.
K_u	kurtosis.
l_x, l_y	lag in mm in flow and transverse direction, respectively.
m, n	variables.
M, N	number of measuring points of bed elevations in x and y direction.
p	order of the structure function.
Q_a	armoring discharge.
R	correlation function.
S_k	skewnesss.
t	time.
x, y	spatial coordinates in flow and transverse direction, respectively.
δx, δy	sampling interval in flow and transverse direction, respectively.
τ_0	bed shear stress.
σ_z	standard deviation of bed elevations.
ξ_p	scaling exponent

[43] **Acknowledgments.** This study was funded by the Deutsche Forschungsgemeinschaft (DFG, grant DI 651/4-2). K. Koll, A. Dittrich, and R. Spigel provided useful comments and suggestions. U. Ecklebe

provided technical support. The writers are grateful to three reviewers and the Associate Editor for helpful comments and suggestions.

References

Aberle, J. (2000), Untersuchung der Rauheitsstruktur zur Bestimmung des Fließwiderstandes in Gebirgsbächen unter Klarwasserabfluß, dissertation, Univ. Karlsruhe, Karlsruhe, Germany.

Aberle, J., and K. Koll (2004), Double-averaged flow field over static armor layers, in *Proceedings of the International Conference on Fluvial Hydraulics River Flow 2004*, vol. 1, edited by M. Greco et al., pp. 225–233, A. A. Balkema, Brookfield, Vt.

Aberle, J., and G. M. Smart (2003), The influence of roughness structure on flow resistance in mountain streams, *J. Hydraul. Res.*, *41*(3), 259–269.

Adams, J. (1979), Gravel size analysis from photographs, *J. Hydraul. Div.*, *105*(10), 1247–1255.

Allen, J. R. L. (1982), *Sedimentary Structures*, *Dev. Sedimentol.*, vol. 30A–30B, Elsevier, New York.

Baiamonte, G., and V. Ferro (1997), The influence of roughness geometry and Shields parameter on flow resistance in gravel-bed channels, *Earth Surf. Processes Landforms*, *22*, 759–772.

Bathurst, J. C. (1978), Flow resistance of large-scale roughness, *J. Hydraul. Div. Am. Soc. Civ. Eng.*, *104*(HY12), 1587–1603.

Bathurst, J. C. (1985), Flow resistance estimation in mountain rivers, *J. Hydraul. Eng.*, *111*(4), 625–643.

Bergeron, N. E. (1996), Scale-space analysis of stream-bed roughness in coarse gravel-bed streams, *Math. Geol.*, *28*(5), 537–561.

Bray, D. I. (1982), Flow resistance in gravel bed rivers, in *Gravel-Bed Rivers*, edited by R. D. Hey et al., pp. 109–133, John Wiley, Hoboken, N. J.

Bunte, K., and S. R. Abt (2001), Sampling surface and subsurface particle-size distributions in wadable gravel- and cobble-bed streams for analyses in sediment transport, hydraulics, and streambed monitoring, *Gen. Tech. Rep. RMRS-GTR-74*, U.S. Dep. of Agric., For. Serv., Rocky Mt. Res. Stn., Fort Collins, Colo.

Butler, J. B., S. N. Lane, and J. H. Chandler (2001), Characterization of the structure of river-bed gravels using two-dimensional fractal analysis, *Math. Geol.*, *33*(3), 301–330.

Carney, S. K., B. P. Bledsoe, and D. Gessler (2006), Representing the bed roughness of coarse-grained streams in computational fluid dynamics, *Earth Surf. Processes Landforms*, *31*, 736–749, doi:10.1002/esp.1274.

Clifford, N. J., A. Robert, and K. S. Richards (1992), Estimation of flow resistance in gravel-bedded rivers: A physical explanation of the multiplier of roughness length, *Earth Surf. Processes Landforms*, *17*, 111–126.

de Jong, C. (1995), Temporal and spatial interactions between river bed roughness, geometry, bedload transport and flow hydraulics in mountain streams—Examples from Squaw Creek (Montana, USA) and Lainbach/Schmiedlaine (upper Bavaria, Germany), *Berlin. Geogr. Abh.*, *59*, 1–229.

Fehr, R. (1987), Geschiebeanalysen in Gebirgsflüssen, *Mitt. Versuchsanst. Wasserbau Hydrol. Glaziol.*, *92*, ETH Zürich, Switzerland.

Ferro, V. (1999), Friction factor for gravel-bed channel with high boulder concentration, *J. Hydraul. Eng.*, *125*(7), 771–778.

Fraccarollo, L., and A. Marion (1995), Statistical approach to bed-material surface sampling, *J. Hydraul. Eng.*, *121*(7), 540–545.

Frisch, U. (1995), *Turbulence, The Legacy of A. N. Kolmogorov*, Cambridge Univ. Press, New York.

Furbish, D. J. (1987), Conditions for geometric similarity of coarse stream-bed roughness, *Math. Geol.*, *19*(4), 291–307.

Goring, D., V. Nikora, and I. K. McEwan (1999), Analysis of the texture of gravel beds using 2-D structure functions, in *River, Coastal, and Estuarine Morphodynamics: Proceedings of the IAHR Symposium*, vol. 2, edited by G. Seminara and P. Blondeaux et al., pp. 111–120, Springer, New York.

Graf, W. (1991), Flow resistance over a gravel bed: Its consequence on initial sediment movement, in *Fluvial Hydraulics of Mountain Regions*, *Lect. Notes Earth Sci.*, vol. 37, edited by A. Armanini and G. Di Silvio, pp. 17–32, Springer, New York.

Griffiths, G. A. (1989), Form resistance in gravel channels with mobile beds, *J. Hydraul. Eng.*, *115*(3), 340–355.

Günter, A. (1971), Die kritische mittlere Sohlenschubspannung bei Geschiebemischungen unter Berücksichtigung der Deckschichtbildung und der turbulenzbedingten Sohlschubspannungsschwankungen, dissertation, ETH Zürich, Zürich, Switzerland.

Hardy, R. J., S. N. Lane, M. R. Lawless, J. L. Best, A. H. Elliott, and D. B. Ingham (2005), Development and testing of a numerical code for treatment of complex river channel topography in three-dimensional CFD models with structured grids, *J. Hydraul. Res.*, *43*(5), 468–480.

Hey, R. D. (1979), Flow Resistance in Gravel-Bed Rivers, *J. Hydraul. Div. Am. Soc. Civ. Eng.*, *105*(HY4), 365–379.

Komar, P. D., and Z. Li (1986), Pivoting analysis of the selective entrainment of sediments by shape and size with applications to gravel threshold, *Sedimentology*, *33*, 425–436.

Kreyszig, E. (1991), *Statistische Methoden und ihre Anwendungen*, Vandenhoeck and Ruprecht, Göttingen, Germany.

Lane, S. N., R. J. Hardy, L. Elliott, and D. B. Ingham (2004), Numerical modeling of flow processes over gravelly surfaces using structured grids and a numerical porosity treatment, *Water Resour. Res.*, *40*, W01302, doi:10.1029/2002WR001934.

Marion, A., S. J. Tait, and I. K. McEwan (2003), Analysis of small-scale gravel bed topography during armoring, *Water Resour. Res.*, *39*(12), 1334, doi:10.1029/2003WR002367.

Monzavi, M. T. (1972), Widerstandsgesetz auf statistischer Basis für extreme und natürliche Rauhigkeiten in Druckrohren, *Tech. Ber. 8*, Inst. für Hydraul. und Hydrol., Darmstadt, Germany.

Nikora, V. (2005), High-order structure functions for planet surfaces: a turbulence metaphor, *IEEE Geosci. Remote Sens. Lett.*, *2*(3), 362–365.

Nikora, V., and J. Walsh (2004), Water-worked gravel surfaces: High-order structure functions at the particle scale, *Water Resour. Res.*, *40*, W12601, doi:10.1029/2004WR003346.

Nikora, V. I., O. I. Nikora, D. A. Noever, and G. M. Smart (1994), New method of structural functions for analyzing fractal scaling properties of natural processes, *J. Phys. A*, *27*, L403–L409.

Nikora, V., D. Goring, and B. J. F. Biggs (1998), On gravel-bed roughness characterization, *Water Resour. Res.*, *34*(3), 517–527.

Nikuradse, J. (1933), Strömungsgesetze in rauhen Rohren, *Forsch. Arb. Ing.*, 361.

Robert, A. (1988), Statistical properties of sediment bed profiles in alluvial channels, *Math. Geol.*, *20*(3), 205–223.

Robert, A. (1990), Boundary roughness in coarse-grained channels, *Prog. Phys. Geogr.*, *14*(1), 42–70.

Robert, A. (1991), Fractal properties of simulated bed profiles in coarse-grained channels, *Math. Geol.*, *23*(3), 367–382.

Schlichting, H., and K. Gersten (1997), *Grenzschicht-Theorie*, *9 Auflage*, Springer, New York.

Smart, G. M., J. Aberle, M. Duncan, and J. Walsh (2004), Measurement and analysis of alluvial bed roughness, *J. Hydraul. Res.*, *42*(3), 227–237.

Vogel, S. (2003), Ansätze zur Bemessung rauer Rampen in aufgelöster Bauweise, *Mitt. Inst. Wasser.*, 88.

Wiberg, P. L., and J. D. Smith (1991), Velocity distribution and bed roughness in high-gradient streams, *Water Resour. Res.*, *27*(5), 825–838.

Wolman, M. G. (1954), A method of sampling coarse river-bed material, *Eos Trans. AGU*, *35*(6), 951–956.

J. Aberle, Leichtweiss-Institute for Hydraulic Engineering, Technical University of Braunschweig, Beethovenstr. 51a, D-38106 Braunschweig, Germany. (j.aberle@tu-bs.de)

V. Nikora, Engineering Department, Fraser Noble Building, Kings College, University of Aberdeen, Aberdeen AB24 3UE, UK. (v.nikora@abdn.ac.uk)